Mathematical Biosciences and Engineering

http://www.aimspress.com/journal/MBE

MBE, 17(6): 6720–6736.
DOI: 10.3934/mbe.2020350
Received: 31 May 2020
Accepted: 16 September 2020
Published: 30 September 2020

Research article

Analysis of a multiscale HIV-1 model coupling within-host viral dynamics and between-host transmission dynamics

Yuyi Xue and Yanni Xiao*

School of Mathematics and Statistics, Xi′an Jiaotong University, Xi′an 710049, China

* **Correspondence:** Email: yxiao@mail.xjtu.edu.cn; Tel: +862982663156; Fax: +862982663156.

Abstract: There are many challenges to constitute the linkage from the macroscale to the microscale and analyze the multiscale model. We proposed a bidirectional coupling model with standard incidence which includes the interaction of between-host transmission dynamics and within-host viral dynamics, and investigated the dynamic behaviors of the multiscale system on two time-scales. We found that the multiscale system exhibits more complex dynamics including backward bifurcation, which means that the usual thresholds for infection control or virus elimination obtained from the epidemiological model or virus dynamic model may not act as threshold parameter under a certain condition. There may be multiple epidemic equilibriums, one of which is stable, although the basic reproduction number is less than 1. We numerically examine the synergistic impact between the macro and micro dynamics. In particular, increasing the drug efficacy can decrease the prevalence of disease. The contact rate may affect the number and size of equilibria of viral dynamics model by inducing the occurrence of backward bifurcation. The finding suggests that the effective control measures may include both the reduction in contact rate or transmission rate at the population level and the increase in drug efficacy at the individual level, and using these control measures together can effectively control the diseases.

Keywords: multiscale model; standard incidence; threshold dynamics; backward bifurcation

1. Introduction

A number of mathematical models of infectious diseases (e.g., human immunodeficiency virus (HIV)) have been studied at a single microscale or macroscale [1–5]. The single-scale models are proposed to either explore the within-host viral dynamics at the individual level and give guides for treatment strategies, or the between-host transmission dynamics at the population level to predict the future prevalence and suggest effective control measures. However, more evidence indicated that viral load at the individual level affects the progression of infection [6, 7]. Laith J et al. found that a higher circulating viral load was positively related to a higher rate of host-to-host transmission [8]. This

means that the dynamics at different scales are not independent, but interrelated. Obviously, this also complicates disease control. For example, implementing measures to change behavior patterns may not only affect the disease transmission at the population level, but even the probability of an individual receiving treatment, and further the within-host virus dynamics. Therefore, formulating a multiscale model that can combine the within-host and between-host scales and study the macro-micro interaction mechanism is significant for determining more effective strategies at different levels.

In recent years, many multiscale systems have been proposed in the area of mathematical biology [9–13]. Initially, some researchers built nested models to consider the evolution of the host and parasite by evolutionary dynamics [14, 15]. Further, researchers applied coupled models to study infectious diseases. They integrated the within-host model into the epidemiological model by introducing the viral load-dependent transmission rate or disease-induced mortality rate to explore the potential effect of micro dynamics on the macro dynamics, design the coupled optimal scheme and provide the cost-effectiveness analysis [16–18]. Later, Feng et al. formulated a multiscale model with an environment compartment to investigate the effects of between-host dynamics on the viral progression within the hosts [19, 20]. Taking contaminated environment as a coupling link, Wang et al. coupled the age-structured macro model and the micro within-host dynamics model through the bacteria-dependent indirect transmission [21], Sun et al. proposed a multiscale model with threshold control strategy to study the effect of threshold-dependent interventions on the spread of infectious disease [22], Xiao et al. linked the macroscale to the microscale in a spatiotemporal context to examine effects of an individual movement and spatial control measures on a disease outbreak [23].

It should be noted that most of the above-mentioned multiscale models were formulated by linking viral dynamics to between-host transmission dynamics, which can not reflect the influence of transmission of disease on viral loads within the hosts. It is worth noting that for some environmentally-driven infectious disease such as Toxoplasma gondii, there have been models successfully coupling the macro level to the microscale [19–21]. However, for some infectious diseases such as HIV that the virus can be spread by direct contact with infected individuals, how to construct a bridge which can couple the epidemiological model to the virus dynamics model and study the interactions between macro and micro level remain unclear and fall within the scope of our study.

The main purpose of this study is to propose a multiscale model which can bidirectionally couple the within-host viral dynamics and between-host transmission dynamics, and then analyze the dynamic behaviors of the full system. Note that most existing coupled models provided that between-host transmission rate is bilinear incidence, which is inconsistent with the fact that one can only contact with limited persons in a certain time. Hence, we include the standard incidence in our study. Specifically, in this article, we first formulate a multiscale model with standard incidence in section 2. In section 3 and section 4, we analyze the dynamic behaviors of the fast subsystem and slow subsystem, which can help us understand the dynamics of the full system. In section 5, we discuss the interactions of within-host and between-host dynamics by a series of numerical simulations. Finally, the main conclusions are highlighted.

2. Model formulation

Here, we take HIV viral dynamics and transmission dynamics as an example to illustrate how we form the links on macro and micro levels. The micro system is embedded into the macro system by

incorporating the viral load-dependent transmission and disease-induced mortality. The virus shed by the contacted infections, depending on the contact rate and prevalence, enter into the within-host viral system due to close contact and act as a bridge such that between-host system is coupled into the within-host system, inspired by the ideas by Kostova [24], Bhattacharya and Maia Martcheva [25]. In order to investigate the impact of macro epidemic dynamics on micro virus dynamics and vice verse, we proposed a multiscale model, motivated by the sexual contact transmission of HIV [26]. The model equations are as follows.

$$\begin{cases} \frac{dS}{dt} = \Pi - c_1\beta_1(V)\frac{S}{N}I - c_2\beta_2(V)\frac{S}{N}A - \mu S, \\ \frac{dI}{dt} = c_1\beta_1(V)\frac{S}{N}I + c_2\beta_2(V)\frac{S}{N}A - (\mu + \xi + \alpha_1(V))I, \\ \frac{dA}{dt} = \xi I - (\mu + \alpha_2(V))A, \\ \frac{dT}{dt} = \lambda - k(1-\eta)TV - dT, \\ \frac{dT^*}{dt} = k(1-\eta)TV - \delta T^*, \\ \frac{dV}{dt} = c_1 p_1 \frac{I}{N} + c_2 p_2 \frac{A}{N} + N_1\delta T^* - cV, \end{cases} \tag{2.1}$$

where $S(t), I(t), A(t)$ are the number of susceptibles, HIV-positive individuals without clinical manifestation and AIDS patients who have developed one or more opportunistic infections regardless of their CD4 count, $N(t) = S(t) + I(t) + A(t)$. $T(t), T^*(t)$, $V(t)$ denote the densities of healthy T cells, infected T cells and viral load, respectively. λ, k, d represent the recruitment, per-capita infection rate, per-capital mortality of healthy cells, δ is the per-capital mortality of infected cells. η is the drug efficacy ($0 \leq \eta \leq 1$). For HIV infection, it represents the effectiveness of reverse transcriptase (RT) inhibitors. N_1 is the virus production rate by an infected cell, c is the clearance rate of virus within host. c_1, c_2 represent the average number of contacts with HIV-positive individuals and AIDS patients who have developed clinical symptoms, p_1, p_2 denote the amount of virus released by HIV infections and AIDS patients at each contact. Π, μ denote recruitment rate and natural death rate of hosts. ξ is the transfer rate from HIV-positive stage to the onset of opportunistic infections. $\beta_1(V), \beta_2(V)$ are the transmission probability of HIV-positive individuals and AIDS patients, $\alpha_1(V), \alpha_2(V)$ are the corresponding disease-related mortality. They are dependent on the viral loads, such as $\beta(V) = aV$, or $\beta(V) = \frac{aV}{1+bV}$, or $\beta(V) = aV^q$, $q < 1$ with

$$\beta(0) = 0, \beta(V) \geq 0, \beta'(V) > 0, \beta''(V) \leq 0.$$

Since the system (2.1) contains the dynamics on different time-scales, i.e., within-host dynamics on a fast time-scale and between-host dynamics on a slow time-scale, it is a challenge to directly study the multiscale system. For this problem, some studies analyzed the full system on two time-scales, i.e., fast system and slow system [27, 28]. The fast system is obtained by assuming that the slow variables are all constants and the slow system is defined by assuming that the fast system will tend to the stable equilibrium very quickly. This methods allows us to derive the analytical results and reveal some meaningful phenomena of the full system from the analyses of the fast and slow subsystems.

3. Dynamics of the fast subsystem

For the within-host system to have a meaningful couple with the between-host system, we focus on the case $I, A > 0$ in the following analysis. We first introduce a slow time-scale $\tau = \epsilon t$ with $0 < \epsilon \ll 1$

and let

$$\Pi = \epsilon\bar{\Pi}, \mu = \epsilon\bar{\mu}, \xi = \epsilon\bar{\xi}, \alpha_1(V) = \epsilon\bar{\alpha}_1(V), \alpha_2(V) = \epsilon\bar{\alpha}_2(V), \beta_1(V) = \epsilon\bar{\beta}_1(V), \beta_2(V) = \epsilon\bar{\beta}_2(V).$$

Then the system (2.1) can be written as

$$\begin{cases} \frac{dS}{dt} = \epsilon[\bar{\Pi} - c_1\bar{\beta}_1(V)\frac{S}{N}I - c_2\bar{\beta}_2(V)\frac{S}{N}A - \bar{\mu}S], \\ \frac{dI}{dt} = \epsilon[c_1\bar{\beta}_1(V)\frac{S}{N}I + c_2\bar{\beta}_2(V)\frac{S}{N}A - (\bar{\mu} + \bar{\xi} + \bar{\alpha}_1(V))I], \\ \frac{dA}{dt} = \epsilon[\bar{\xi}I - (\bar{\mu} + \bar{\alpha}_2(V))A], \\ \frac{dT}{dt} = \lambda - k(1-\eta)TV - dT, \\ \frac{dT^*}{dt} = k(1-\eta)TV - \delta T^*, \\ \frac{dV}{dt} = c_1p_1\frac{I}{N} + c_2p_2\frac{A}{N} + N_1\delta T^* - cV. \end{cases}$$

Setting $\epsilon = 0$ and $\frac{d}{dt} = \cdot$, we get the fast subsystem

$$\begin{cases} \dot{T} = \lambda - k(1-\eta)TV - dT, \\ \dot{T}^* = k(1-\eta)TV - \delta T^*, \\ \dot{V} = c_1p_1\frac{\hat{I}}{\hat{N}} + c_2p_2\frac{\hat{A}}{\hat{N}} + N_1\delta T^* - cV, \end{cases} \tag{3.1}$$

where $\hat{I}, \hat{A}$ are considered as constants. Let $E_f^* = (\tilde{T}^*, \tilde{V}, \tilde{T})$ denote a positive equilibrium of system (3.1). It is obvious that for $\hat{I} > 0$, the fast subsystem (3.1) has no disease-free equilibrium. In addition, we can get the following result.

Theorem 1 For $\hat{I} > 0$, the fast subsystem (3.1) has unique positive equilibrium E_f^*, which is globally asymptotically stable.

Proof. Let the right sides of system (3.1) be equal to 0 and then we get $\tilde{T}^* = \frac{\lambda - d\tilde{T}}{\delta}, \tilde{V} = \frac{(c_1p_1\hat{I}/\hat{N} + c_2p_2\hat{A}/\hat{N}) + N_1(\lambda - d\tilde{T})}{c}$ and $\tilde{T}$ satisfying

$$a_0\tilde{T}^2 + a_1\tilde{T} + a_2 = 0,$$

where $a_0 = k(1-\eta)N_1d, a_1 = -[k(1-\eta)(N_1\lambda + c_1p_1\hat{I}/\hat{N} + c_2p_2\hat{A}/\hat{N}) + cd], a_2 = c\lambda$.

Solving the above equation, we get

$$\tilde{T}_1 = \frac{-a_1 + \sqrt{a_1^2 - 4a_0a_2}}{2a_0}, \tilde{T}_2 = \frac{-a_1 - \sqrt{a_1^2 - 4a_0a_2}}{2a_0}$$

with $a_1^2 - 4a_0a_2 > 0$. Obviously, $\tilde{T}_1 > \tilde{T}_2 > 0$. For a positive equilibrium, it should satisfy $\tilde{T}^*, \tilde{V} > 0$, which corresponds to the condition $\tilde{T} < \frac{\lambda}{d}$. It is easy to verify $\tilde{T}_2 < \frac{\lambda}{d} < \tilde{T}_1$. Hence, the system (3.1) has unique positive equilibrium $E_f^* = (\tilde{T}^*, \tilde{V}, \tilde{T})$ with $\tilde{T} = \tilde{T}_2$. This completes the proof.

In the following, we verify that E_f^* is globally asymptotically stable. Formulating the following Lyapunov function

$$W(T, T^*, V) = (T - \tilde{T} - \tilde{T}ln\frac{T}{\tilde{T}}) + (T^* - \tilde{T}^* - \tilde{T}^*ln\frac{T^*}{\tilde{T}^*}) + \frac{1}{N_1}(V - \tilde{V} - \tilde{V}ln\frac{V}{\tilde{V}}),$$

then the derivative of $W(t)$ is

$$\begin{aligned}\frac{dW}{dt} =&(1-\frac{\tilde{T}}{T})[\lambda - k(1-\eta)TV - dT] + (1-\frac{\tilde{T}^*}{T^*})[k(1-\eta)TV - \delta T^*] + \frac{1}{N_1}(1-\frac{\tilde{V}}{V})(c_1p_1\frac{\hat{I}}{\hat{N}} + c_2p_2\frac{\hat{A}}{\hat{N}} + \\ & N_1\delta T^* - cV) \\ =&d\tilde{T}(2-\frac{T}{\tilde{T}}-\frac{\tilde{T}}{T}) + \delta\tilde{T}^*(3-\frac{\tilde{T}}{T}-\frac{\tilde{V}T^*}{\tilde{T}^*V}-\frac{\tilde{T}^*TV}{\tilde{T}\tilde{V}T^*}) + \frac{c_1p_1\hat{I}/\hat{N} + c_2p_2\hat{A}/\hat{N}}{N_1}(2-\frac{V}{\tilde{V}}-\frac{\tilde{V}}{V}) \\ \leq&0\end{aligned}$$

and for all $T, T^*, V > 0$, $\frac{dW}{dt} = 0$ holds only at E_f^*. By LaSalle's invariant principle, E_f^* is globally asymptotically stable.

4. Dynamics of the slow subsystem

Writing system (2.1) with respect to the slow time-scale τ, we have

$$\begin{cases} \frac{dS}{d\tau} = \bar{\Pi} - c_1\bar{\beta}_1(V)\frac{S}{N}I - c_2\bar{\beta}_2(V)\frac{S}{N}A - \bar{\mu}S, \\ \frac{dI}{d\tau} = c_1\bar{\beta}_1(V)\frac{S}{N}I + c_2\bar{\beta}_2(V)\frac{S}{N}A - (\bar{\mu}+\bar{\xi}+\bar{\alpha}_1(V))I, \\ \frac{dA}{d\tau} = \bar{\xi}I - (\bar{\mu}+\bar{\alpha}_2(V))A, \\ \epsilon\frac{dT}{d\tau} = \lambda - k(1-\eta)TV - dT, \\ \epsilon\frac{dT^*}{d\tau} = k(1-\eta)TV - \delta T^*, \\ \epsilon\frac{dV}{d\tau} = c_1p_1\frac{I}{N} + c_2p_2\frac{A}{N} + N_1\delta T^* - cV. \end{cases}$$

Letting $\epsilon = 0$, $\frac{d}{d\tau} = '$, and dropping the bar for convenience, we obtain the slow subsystem

$$\begin{cases} S' = \Pi - c_1\beta_1(\tilde{V})\frac{I}{N}S - c_2\beta_2(\tilde{V})\frac{A}{N}S - \mu S, \\ I' = c_1\beta_1(\tilde{V}))\frac{I}{N}S + c_2\beta_2(\tilde{V})\frac{A}{N}S - (\mu+\xi+\alpha_1(\tilde{V}))I, \\ A' = \xi I - (\mu+\alpha_2(\tilde{V}))A, \end{cases} \tag{4.1}$$

where $\tilde{V}(S, I, A)$ is the steady state of the fast subsystem. The initial condition for system (4.1) is $S_0 > 0$, I_0 or $A_0 > 0$.

By using the next generation method [29], we can calculate the basic reproduction number of the slow system (4.1) as follows

$$R_s = \frac{(\mu+\alpha_2(\tilde{V}(0)))c_1\beta_1(\tilde{V}(0)) + \xi c_2\beta_2(\tilde{V}(0))}{(\mu+\xi+\alpha_1(\tilde{V}(0)))(\mu+\alpha_2(\tilde{V}(0)))},$$

where

$$\tilde{V}(0) = \lim_{I,A\to 0}\tilde{V}(S, I, A) = \frac{N_1\lambda}{c}(1-\frac{1}{R_f}),$$

with $R_f > 1$. Here, $R_f = \frac{\lambda N_1 k(1-\eta)}{cd}$ represents the basic reproduction number of isolated within-host system.

4.1. Stability of disease-free equilibrium

In the following, we first analyze the stability of disease-free equilibrium for the slow subsystem (4.1).

Theorem 2 The disease-free equilibrium $E_0^s = (\frac{\Pi}{\mu}, 0, 0)$ of slow subsystem (4.1) is locally asymptomatically stable (LAS) for $R_s < 1$ and unstable for $R_s > 1$.

Proof. The characteristic equation of Jacobian matrix at E_0^s is

$$(\chi+\mu)\{\chi^2 + [2\mu+\xi+\alpha_1(\tilde{V}(0))+\alpha_2(\tilde{V}(0))-c_1\beta_1(\tilde{V}(0))]\chi + [(\mu+\xi+\alpha_1(\tilde{V}(0)))(\mu+\alpha_2(\tilde{V}(0)))-(\mu+\alpha_2(\tilde{V}(0)))c_1\beta_1(\tilde{V}(0))-\xi c_2\beta_2(\tilde{V}(0))]\} = 0.$$

It is easy obtained

$$\chi_1 = -\mu,$$
$$\chi_2\chi_3 = (\mu+\xi+\alpha_1(\tilde{V}(0)))(\mu+\alpha_2(\tilde{V}(0)))(1-R_s),$$
$$\chi_2+\chi_3 = (\mu+\xi+\alpha_1(\tilde{V}(0)))(R_s - 1 - \frac{\mu+\alpha_2(\tilde{V}(0))}{\mu+\xi+\alpha_1(\tilde{V}(0))} - \frac{\xi c_2\beta_2(\tilde{V}(0))}{(\mu+\xi+\alpha_1(\tilde{V}(0)))(\mu+\alpha_2(\tilde{V}(0)))}).$$

Obviously, for $R_s < 1$, $\chi_2+\chi_3 < 0$ and $\chi_2\chi_3 > 0$, that is $\chi_2 < 0, \chi_3 < 0$. Thus, the disease-free equilibrium is locally asymptomatically stable. For $R_s > 1$, $\chi_2\chi_3 < 0$, i.e., there is a positive solution for above characteristic equation. This demonstrates the disease-free equilibrium is unstable. Hence, we obtain the Theorem 2.

4.2. Existence and number of positive equilibrium

If there exists the equilibrium for the slow subsystem, we let $E_s^* = (\tilde{S}, \tilde{I}, \tilde{A})$ denote a positive equilibrium of system (4.1). For the existence and stability of the endemic equilibrium, it is always difficult to be analyzed theoretically with viral load-dependent transmission rate, disease-induced mortality rate and standard incidence, simultaneously. Hence, we provide partial analytic proofs for the case where $\beta_i(V)$ satisfies the properties as mentioned in the Section 2 and $\alpha_i(V) = \alpha_i$ $(i = 1, 2)$. Then we extend the results with numerical simulations.

Let $\tilde{x}_1 = c_1p_1\frac{\tilde{I}}{\tilde{N}} + c_2p_2\frac{\tilde{A}}{\tilde{N}}$, then the equilibrium of the fast subsystem can be written as

$$\tilde{T}^* = \frac{\lambda - d\tilde{T}}{\delta},$$
$$\tilde{V} = \frac{\tilde{x}_1 + N_1(\lambda - d\tilde{T})}{c},$$
$$\tilde{T} = \frac{(k(1-\eta)\tilde{x}_1 + k(1-\eta)N_1\lambda + cd) - \sqrt{(k(1-\eta)\tilde{x}_1 + k(1-\eta)N_1\lambda + cd)^2 - 4N_1dk(1-\eta)\lambda c}}{2N_1dk(1-\eta)}.$$

Let $\tilde{x}_2 = c_1\beta_1(\tilde{V})\frac{\tilde{I}}{\tilde{N}} + c_2\beta_2(\tilde{V})\frac{\tilde{A}}{\tilde{N}}$, then the equilibrium E_s^* of the slow subsystem can be written as

$$\tilde{I} = \frac{\Pi\tilde{x}_2}{(\mu+\xi+\alpha_1)(\mu+\tilde{x}_2)}, \tilde{A} = \frac{\xi\tilde{I}}{\mu+\alpha_2}, \tilde{S} = \frac{\Pi - (\mu+\xi+\alpha_1)\tilde{I}}{\mu},$$
$$\tilde{N} = \tilde{I} + \tilde{A} + \tilde{S} = \frac{\Pi\{(\mu+\alpha_2)(\mu+\xi+\alpha_1)(\mu+\tilde{x}_2) - [\xi\alpha_2 + \alpha_1(\mu+\alpha_2)]\tilde{x}_2\}}{\mu(\mu+\alpha_2)(\mu+\xi+\alpha_1)(\mu+\tilde{x}_2)}.$$

Further, $\tilde{x}_1$ can be described by $\tilde{x}_2$, that is

$$\tilde{x}_1 = \frac{[(\mu+\alpha_2)c_1p_1 + \xi c_2p_2]\mu\tilde{x}_2}{(\mu+\alpha_2)(\mu+\xi+\alpha_1)(\mu+\tilde{x}_2) - [\xi\alpha_2 + \alpha_1(\mu+\alpha_2)]\tilde{x}_2}.$$

Thus, $\tilde{T} = \tilde{T}(\tilde{x}_2), \tilde{T}^* = \tilde{T}^*(\tilde{x}_2), \tilde{V} = \tilde{V}(\tilde{x}_2)$. Using the equation $\tilde{x}_2 = c_1\beta_1(\tilde{V})\frac{\tilde{I}}{\tilde{N}} + c_2\beta_2(\tilde{V})\frac{\tilde{A}}{\tilde{N}}$, we obtain

$$\tilde{x}_2 = \frac{[(\mu+\alpha_2)c_1\beta_1(\tilde{V}) + \xi c_2\beta_2(\tilde{V})]\mu\tilde{x}_2}{(\mu+\alpha_2)(\mu+\xi+\alpha_1)(\mu+\tilde{x}_2) - [\xi\alpha_2 + \alpha_1(\mu+\alpha_2)]\tilde{x}_2}.$$

Let

$$H(x_2) = \frac{\mu[(\mu+\alpha_2)c_1\beta_1(\tilde{V}(x_2)) + \xi c_2\beta_2(\tilde{V}(x_2))]}{(\mu+\alpha_2)(\mu+\xi+\alpha_1)(\mu+x_2) - [\xi\alpha_2 + \alpha_1(\mu+\alpha_2)]x_2} - 1, \tag{4.2}$$

then $\tilde{x}_2$ is the solution of equation $H(x_2) = 0$. In the following, we only need to identify the number of zeros of $H(x_2)$ for $x_2 \geq 0$ by examining the properties of the function H. It can be verified that

$$H(0) = \frac{[(\mu+\alpha_2)c_1\beta_1(\tilde{V}(0)) + \xi c_2\beta_2(\tilde{V}(0))]}{(\mu+\alpha_2)(\mu+\xi+\alpha_1)} - 1 = R_s - 1 = \begin{cases} < 0, \text{for } R_f > 1, R_s < 1, \\ > 0, \text{for } R_f > 1, R_s > 1, \\ -1, \text{for } R_f < 1, \end{cases}$$

and $H(\infty) < 0$.

The derivative of $H(x_2)$ is

$$H'(x_2) = \frac{\mu G(x_2)}{\{(\mu+\alpha_2)(\mu+\xi+\alpha_1)(\mu+x_2) - [\xi\alpha_2 + \alpha_1(\mu+\alpha_2)]x_2\}^2},$$

where

$$\begin{aligned} G(x_2) = {} & [(\mu+\alpha_2)c_1\beta_1'(\tilde{V}) + \xi c_2\beta_2'(\tilde{V})]\{(\mu+\alpha_2)(\mu+\xi+\alpha_1)(\mu+x_2) - [\xi\alpha_2 + \alpha_1(\mu+\alpha_2)]x_2\}\tilde{V}'(x_2) \\ & - [(\mu+\alpha_2)c_1\beta_1(\tilde{V}) + \xi c_2\beta_2(\tilde{V})]\mu(\mu+\xi+\alpha_2). \end{aligned} \tag{4.3}$$

We find that the sign of $H'(x_2)$ can be determined by $G(x_2)$. So, we first analyze the properties of the function $G(x_2)$.

$$\begin{aligned} G'(x_2) = {} & [(\mu+\alpha_2)c_1\beta_1''(\tilde{V}) + \xi c_2\beta_2''(\tilde{V})]\{(\mu+\alpha_2)(\mu+\xi+\alpha_1)(\mu+x_2) - [\xi\alpha_2 + \alpha_1(\mu+\alpha_2)]x_2\}\tilde{V}'^2(x_2) + \\ & [(\mu+\alpha_2)c_1\beta_1'(\tilde{V}) + \xi c_2\beta_2'(\tilde{V})]\{(\mu+\alpha_2)(\mu+\xi+\alpha_1)(\mu+x_2) - [\xi\alpha_2 + \alpha_1(\mu+\alpha_2)]x_2\}\tilde{V}''(x_2) < 0, \end{aligned}$$

with

$$\tilde{V}'(x_2) = \frac{1}{2c}x_1'(x_2)\left(1 + \frac{k(1-\eta)x_1 + k(1-\eta)N_1\lambda + cd}{\sqrt{(k(1-\eta)x_1 + k(1-\eta)N_1\lambda + cd)^2 - 4N_1dk(1-\eta)\lambda c}}\right) > 0,$$

$$\begin{aligned} \tilde{V}''(x_2) = {} & \tfrac{1}{2c}\{(1 + \tfrac{k(1-\eta)x_1 + k(1-\eta)N_1\lambda + cd}{\sqrt{(k(1-\eta)x_1 + k(1-\eta)N_1\lambda + cd)^2 - 4N_1dk(1-\eta)\lambda c}})x_1'' + [1 - \tfrac{(k(1-\eta)x_1 + k(1-\eta)N_1\lambda + cd)^2}{(k(1-\eta)x_1 + k(1-\eta)N_1\lambda + cd)^2 - 4N_1dk(1-\eta)\lambda c}] \\ & \tfrac{k(1-\eta)x_1'^2}{\sqrt{(k(1-\eta)x_1 + k(1-\eta)N_1\lambda + cd)^2 - 4N_1dk(1-\eta)\lambda c}}\} < 0, \end{aligned}$$

$$x_1'(x_2) = \frac{\mu^2(\mu+\alpha_2)(\mu+\xi+\alpha_1)[c_1p_1(\mu+\alpha_2) + c_2p_2\xi]}{\{(\mu+\alpha_2)(\mu+\xi+\alpha_1)(\mu+x_2) - [\xi\alpha_2 + \alpha_1(\mu+\alpha_2)]x_2\}^2} > 0,$$

$$x_1''(x_2) = \frac{-2\mu^3(\mu+\xi+\alpha_2)(\mu+\alpha_2)(\mu+\xi+\alpha_1)[c_1p_1(\mu+\alpha_2) + c_2p_2\xi]}{\{(\mu+\alpha_2)(\mu+\xi+\alpha_1)(\mu+x_2) - [\xi\alpha_2 + \alpha_1(\mu+\alpha_2)]x_2\}^3} < 0.$$

The result indicates that the function $G(x_2)$ is a monotone decreasing function and $G(\infty) < 0$. Thus, if $G(0) > 0$, then with x_2 increasing, the function $H'(x_2) > 0$ firstly and then $H'(x_2) < 0$, which means

that the function $H(x_2)$ increases firstly and then decreases. In this case, if $H(0) < 0$ and $H_{max} > 0$, we can obtain function $H(x_2)$ has two positive equilibriums; if $H(0) < 0$ and $H_{max} = 0$ or only $H(0) > 0$, there is unique positive equilibrium. If $G(0) < 0$, then the function $H(x_2)$ always decreases. In this case, if $H(0) < 0$, then there is no positive equilibrium; if $H(0) > 0$, then there is only one positive equilibrium. In summary, we give the following results.

Theorem 3 Let $H = H(x_2), G = G(x_2)$ be the function defined in (4.2) and (4.3), $H_{max} = \max_{x_2} H(x_2)$,

(1) For $R_s < 1, R_f > 1$;
  (a) If $G(0) > 0$ and $H_{max} > 0$, there exists two positive equilibriums E_s^{1*}, E_s^{2*};
  (b) If $G(0) > 0$ and $H_{max} = 0$, there is only one positive equilibrium E_s^*;
  (c) If $G(0) \leq 0$ or $H_{max} < 0$, there is no positive equilibrium;
(2) For $R_s > 1, R_f > 1$, there is only one positive equilibrium E_s^*;
(3) For $R_f < 1$;
  (a) If $G(0) > 0$ and $H_{max} > 0$, there exists two positive equilibriums E_s^{1*}, E_s^{2*};
  (b) If $G(0) > 0$ and $H_{max} = 0$, there is only one positive equilibrium E_s^*;
  (c) If $G(0) \leq 0$ or $H_{max} < 0$, there is no positive equilibrium.

To demonstrate that there are corresponding parameter values which can satisfy all conditions described in Theorem 3, we plot the curve $H(x_2)$ for different parameter sets to show the three cases in which H has 0, 1 or 2 zeros, that is the slow subsystem may have 0, 1 or 2 interior equilibriums. In Figure 1(A), we fix most parameters and change R_s by parameter c_2. It shows for $0.5492 < R_s < 1$, the function $H(x_2)$ has two zeros meaning there are two interior equilibriums for slow subsystem, but for $R_s < 0.5492$, there is no positive equilibrium. This result demonstrates $R_s = 0.5492$ is a threshold which determines the number of positive equilibrium. In Figure 1(B), we discuss the case of $R_f < 1$. Most parameters have the same values as those in Figure 1(A) except N_1. We change R_f by parameter N_1. It shows $R_f = 0.7995$ is the lower bound such that the slow subsystem has two interior equilibriums.

4.3. Local stability of the positive equilibrium

In the following analysis, we choose $\beta_i(V) = a_i V, \alpha_i(V) = \alpha_i, i = 1, 2$. Then, the Jacobian matrix of the slow subsystem (4.1) at $E_s^* = (\tilde{S}, \tilde{I}, \tilde{A})$ is

$$J(E_s^*) = \begin{pmatrix} -(u_1+u_2)-\mu & -(u_3+u_4) & -(u_5+u_6) \\ u_1+u_2 & u_3+u_4-(\mu+\xi+\alpha_1) & u_5+u_6 \\ 0 & \xi & -(\mu+\alpha_2) \end{pmatrix},$$

where

$$\begin{aligned} u_1+u_2 &= (\mu+\xi+\alpha_1)\tilde{I}(\tfrac{\tilde{V}_S'}{\tilde{V}} + \tfrac{1}{\tilde{S}} - \tfrac{1}{\tilde{N}}), \\ u_3+u_4 &= (\mu+\xi+\alpha_1)\tilde{I}(\tfrac{\tilde{V}_I'}{\tilde{V}} - \tfrac{1}{\tilde{N}}) + \tfrac{c_1 a_1 \tilde{V}\tilde{S}}{\tilde{N}}, \\ u_5+u_6 &= (\mu+\xi+\alpha_1)\tilde{I}(\tfrac{\tilde{V}_A'}{\tilde{V}} - \tfrac{1}{\tilde{N}}) + \tfrac{c_2 a_2 \tilde{V}\tilde{S}}{\tilde{N}}. \end{aligned}$$

Let $\tilde{y} = 1 + \frac{k(1-\eta)\tilde{x}_1 + k(1-\eta)N_1\lambda + cd}{\sqrt{(k(1-\eta)\tilde{x}_1 + k(1-\eta)N_1\lambda + cd)^2 - 4N_1 dk(1-\eta)}}$, then

$$\tilde{V}_S' = -\frac{1}{2c\tilde{N}}\tilde{x}_1\tilde{y}, \tilde{V}_I' = \frac{1}{2c\tilde{N}}(c_1 p_1 - \tilde{x}_1)\tilde{y}, \tilde{V}_A' = \frac{1}{2c\tilde{N}}(c_2 p_2 - \tilde{x}_1)\tilde{y}.$$

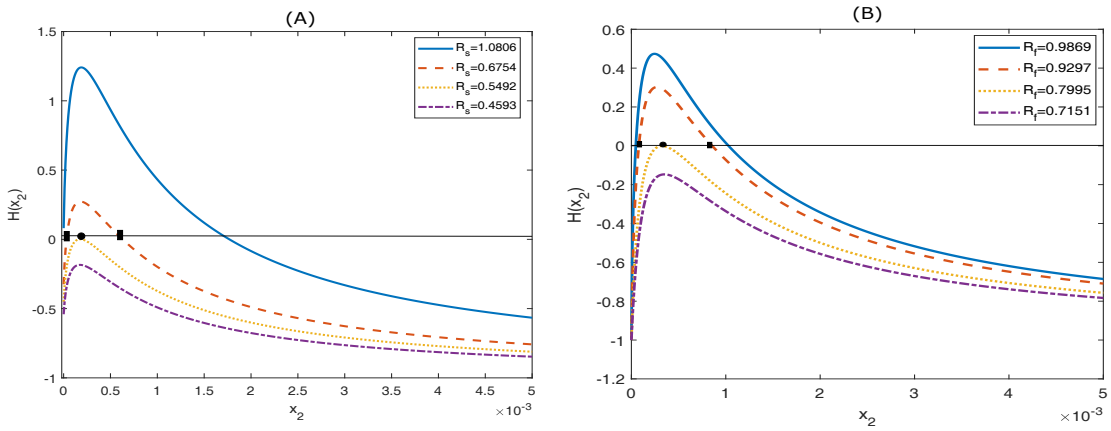

Figure 1. (A) The plot shows the $H(x_2)$ curves for different values of R_s when all other parameter values are fixed except for c_2 with $R_f > 1$. It shows that $H(x_2)$ has two intersections with horizontal axis for $0.5492 < R_s < 1$. (B) The plot shows the $H(x_2)$ curves for different values of R_f when all other parameter values are fixed except for N_1 with $R_f < 1$. It shows $R_f = 0.7995$ is a lower bond such that the slow system has two positive equilibriums. The other parameters in this figure are $\Pi = 4, a_1 = 2 \cdot 10^{-10}, a_2 = 10^{-9}, \mu = 4 \cdot 10^{-4}, \xi = 2 \cdot 10^{-4}, \alpha_1 = 10^{-4}, \alpha_2 = 10^{-6}, d = 0.3, c = 0.02101, \lambda = 60.1, k = 1.5 \cdot 10^{-6}, \eta = 0.5, c_1 = 30, p_1 = 40, p_2 = 60$.

Being similar to above description, $\tilde{I}, \tilde{S}, \tilde{N}, \tilde{x}_1$ can be written as the functions of $\tilde{x_2}$. The characteristic equation of Jacobian matrix at E_s^* is

$$z^3 + j_2 z^2 + j_1 z + j_0 = 0,$$

where

$$j_0 = (\mu + \xi + \alpha_1)(\mu + \alpha_2)(\mu + u_1 + u_2) - \mu(\mu + \alpha_2)(u_3 + u_4) - \mu\xi(u_5 + u_6),$$
$$j_1 = (2\mu + \xi + \alpha_1 + \alpha_2)(\mu + u_1 + u_2) - (2\mu + \alpha_2)(u_3 + u_4) - \xi(u_5 + u_6) + (\mu + \xi + \alpha_1)(\mu + \alpha_2),$$
$$j_2 = 3\mu + \xi + \alpha_1 + \alpha_2 + u_1 + u_2 - u_3 - u_4.$$

According to Routh-Hurwitz criterion, we need to identify the sign of j_0, j_1 and $j_1 j_2 - j_0$. Specifically, if $j_0 < 0$, E_s^* is unstable, whereas if $j_0 > 0$ and $j_1 > 0, j_1 j_2 - j_0 > 0$, E_s^* is locally stability. It is very difficult to theoretically judge the sign of j_i $(i = 1, 2, 3)$, due to the complexity of these functions, so we conduct a large number of numerical simulations. We discover that the Routh-Hurwitz criterion is only satisfied at the larger equilibrium for $R_s < 1, R_f > 1$ and is always satisfied at the unique equilibrium for $R_s > 1, R_f > 1$. We plot the equilibria and the corresponding stability for different cases in Figure 2: blue dashed line represents unstable equilibriums and black solid line denotes stable equilibriums and give the following conjectures: (1) for $R_s < 1, R_f > 1$, if $G(0) > 0$ and $H_{max} > 0$, the larger positive equilibrium is locally asymptotically stable, the other is unstable; (2) for $R_s > 1, R_f > 1$, the unique positive equilibrium is locally asymptotically stable; (3) for $R_f < 1$, if $G(0) > 0$ and $H_{max} > 0$, the larger positive equilibrium is locally asymptotically stable, the other is unstable.

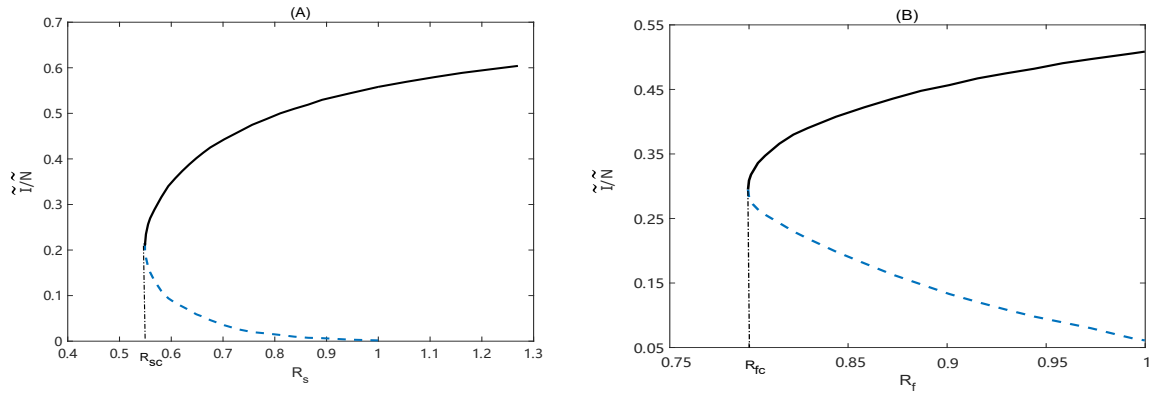

Figure 2. The plots show the fraction of infected individuals at the equilibrium $\tilde{I}/\tilde{N}$ as a function of R_s and R_f. The solid line and dashed line correspond to stable and unstable equilibrium. (A) Changing R_s for the case $R_f > 1$, the backward bifurcation occurs at $R_s = R_{sc} = 0.5492$. If $0.5492 < R_s < 1$, there are two positive equilibriums, one stable, the other unstable. (B) Changing R_f, the backward bifurcation occurs at $R_f = R_{fc} = 0.7995$. There are a stable positive equilibrium and an unstable equilibrium for $R_f \in (0.7995, 1)$.

4.4. Backward bifurcation

We note that the existence of multiple endemic states and their stability may indicate the possibility of a backward bifurcation for our coupled system. In this section, we provide the detailed numerical studies about the parameter regions in which the bifurcation may occur and simulations illustrating the bistability of the disease-free equilibrium and endemic state. We plot the fraction of infected individuals at the positive steady state $\tilde{I}/\tilde{N}$ as a function of R_s and R_f, where the solid and dashed line correspond to the stable and unstable equilibrium, separately. Figure 2(A) shows when $R_s < 1$, there is a lower bound R_{sc} for R_s, above which the system has two positive equilibriums: one is stable, another is unstable and below which the system has no positive equilibria. This denotes the threshold, which governs the eradication of disease, is $R_s = R_{sc} = 0.5492$. In other words, the infectious disease can only be controlled until $R_s < R_{sc}$. This highlights the challenges in the control of disease. Similar to Figure 2(A), Figure 2(B) shows there exists a stable equilibria and an unstable equilibria for $R_f \in (R_{fc}, 1)$, which demonstrates a backward bifurcation can occur for $R_f < 1$. This result suggests that contact with infected individuals may cause the virus to persist in the population, although the virus can be cleared in the isolated individuals.

In Section 3 and 4, we analyze the dynamics of fast and slow subsystems, which are useful to obtain the theoretical results and reveal some meaningful phenomena of the full system. To confirm the analytical results, particularly the threshold condition for various dynamic behaviors of the full system, we plot the solution curve of the full system. Figure 3(A)–(B) show the time series of fraction of infected individuals for the case $R_s < 1, R_f > 1$ and $R_f < 1$, separately. We observe there exists bistable attractors for these two cases. The solutions converge to the disease-free equilibrium with lower initial values of $I(0)$, whereas the solutions converge to the interior equilibrium with higher initial values of $I(0)$. Figure 3(C)–(D) plot the time series of fraction of infected individuals and viral load for the case $R_s > 1, R_f > 1$, in which the system has a unique interior equilibrium. The result shows the two time scales for the fast variable V and slow variable I/N. Specifically, the fast variable V

quickly approaches the value around its equilibrium, followed by the convergence of the slow variable I/N at a slow rate. What's more, it should be noted that for the case $\alpha_1(V) = \alpha_1 V, \alpha_2(V) = \alpha_2 V$ with bilinear incidence, the system may appear richer dynamics except for the backward bifurcation. Specifically, given suitable parameter values for the case $R_s > 1, R_f > 1$, we plot the phase trajectories of the between-host system and the within-host system as shown in Figure 4, in which we can observe the appearance of a stable limit cycle for the full system.

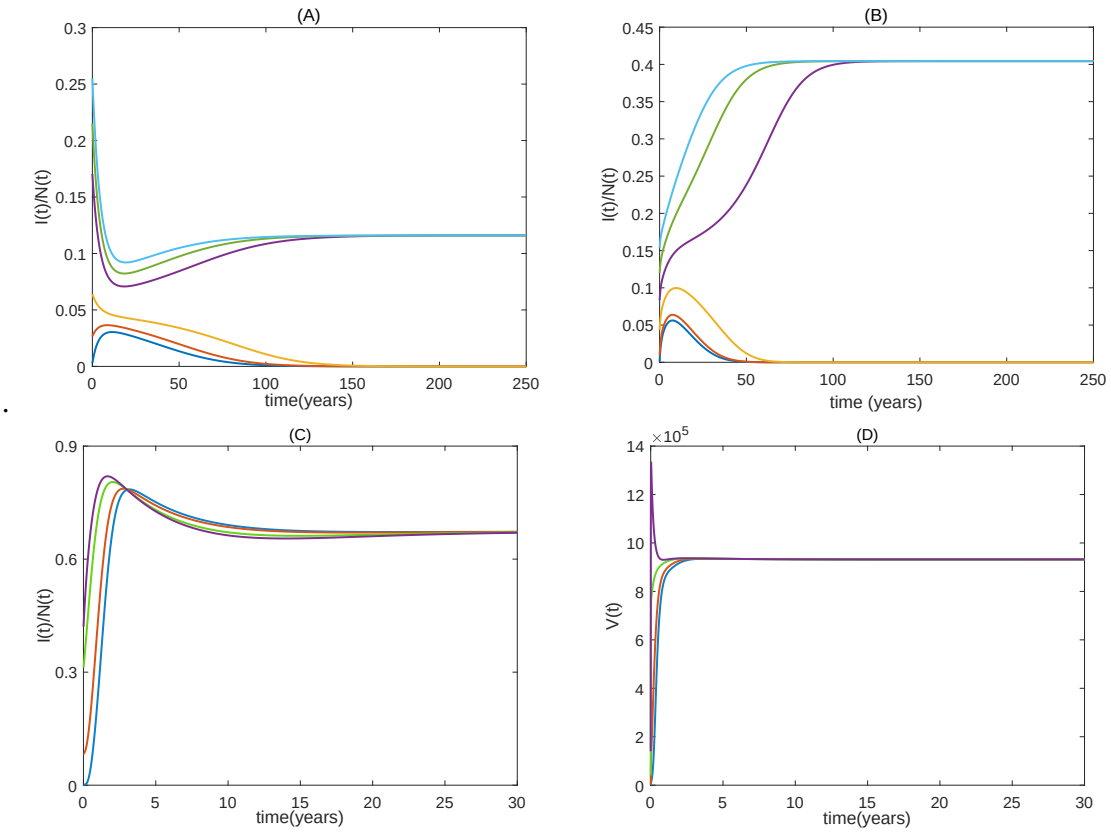

Figure 3. Solution curves of the full system. The time series of fraction of infected individuals $I(t)/N(t)$ for the case (A) $R_s < 1, R_f > 1$; (B) $R_f < 1$. It demonstrates that the solutions converge to disease-free or positive equilibria depending on the initial value. (C)-(D) The time series of fraction of infected individuals $I(t)/N(t)$ and viral load V for the case $R_s > 1, R_f > 1$. The solutions converge to the unique interior equilibrium.

5. The interactions of within-host and between-host systems

In the following, we will discuss the interactions of within-host and between-host dynamics. To explore the influence of macro transmission dynamics on the micro virus dynamics, we plot the viral load at the equilibrium $\tilde{V}$ versus the fraction of infected individuals at equilibrium $\tilde{I}/\tilde{N}$, contact rate c_2 and viral releasing rate per contact p_2. Figure 5(A) shows that $\tilde{V}$ is an increasing function of $\tilde{I}/\tilde{N}$, which demonstrates the more infected individuals in the population, the higher the viral loads. In addition, as R_f increases, $\tilde{V}$ also increases. Figure 5(B) gives the variation in the number and the size of equilibrium $\tilde{V}$ with contact rate c_2 increasing. For the case $R_f = 0.8582 < 1$, there exists a critical level $\bar{c}_2 = 13.6$

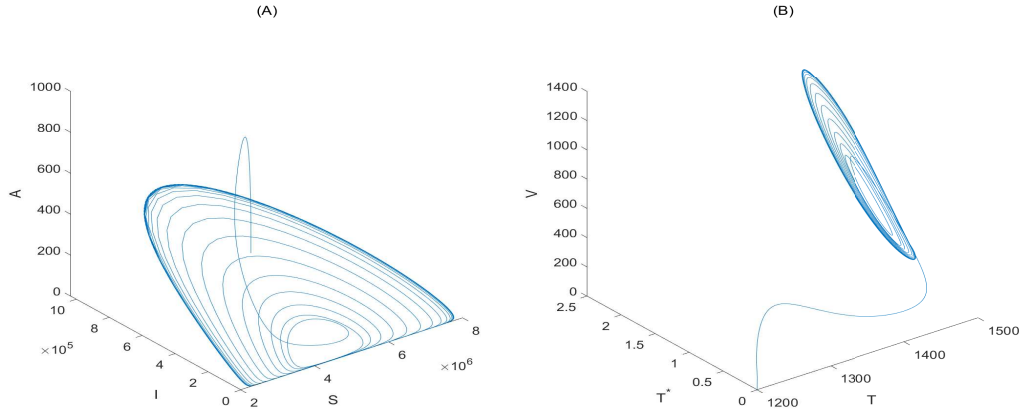

Figure 4. The phase trajectory of the (A) between-host system and (B) the within-host system for the case $\alpha_1(V) = \alpha_1 V, \alpha_2 = \alpha_2 V$ with bilinear incidence. Setting parameters $\Pi = 4.545 * 10^6/365, \mu = 0.0149/365, \xi = 0.116/365, \alpha_1 = 0.318/365, \alpha_2 = 0.172/365, \lambda = 15, d = 0.01, c = 3, k = 2.4 * 10^{-6}, \delta = 0.5, N_1 = 3500, c_1 = 10, c_2 = 5.3, p_1 = 0.00004, p_2 = 0.00004, a_1 = 1.07 * 10^{-11}, a_2 = 1.07 * 10^{-11}, \eta = 0.756$, which corresponds to $R_f = 1.0248 > 1, R_s > 1$.

for contact rate c_2, above which there are two positive equilibriums: one is stable, the other is unstable and below which there is no positive equilibria. Further, for $c_2 > \bar{c}_2$, the larger the contact rate is, the higher the stable equilibrium level of viral loads is. The results suggest that for the coupled within-host dynamic model, $R_f = 1$ is not a threshold to govern the eradication of virus in the hosts. Contact with infected individuals may cause the virus to persist in the population, even if the virus can not be persistent in the isolated individuals. Note that for the case $R_f = 1.1013 > 1$, there is no positive equilibrium $\tilde{V}$ for $c_2 < 5.3$. This result implies that having fewer contacts with infected individuals, the virus will eventually be eliminated at the population level even if there are some individuals who carry virus for long time. Figure 5(C) shows that as viral releasing rate p_2 increases, the value of stable equilibrium $\tilde{V}$ also increases in the case $R_f > 1$. This demonstrates that the final viral loads may tend to high level if contacts occur with infected individuals whose virus replication is in the active period. The results suggest that limiting contact with infected individuals by some protective measures, especially with those whose virus replication is active, is effective to control virus at a low level.

To investigate the influence of micro parameters on the macro disease transmission, we plot the prevalence at equilibrium $\tilde{I}/\tilde{N}$ against drug efficacy η under two cases: case 1): $p_1 = 40, p_2 = 50$ and case 2): $p_1 = p_2 = 0$. In particular, the case 2) with $p_1 = p_2 = 0$ means decoupling the macro dynamics from micro model. With assumption $\alpha_i(V) = \alpha_i$, Figure 5(D) shows that increasing treatment efficacy η leads to the decline of the prevalence $\tilde{I}/\tilde{N}$. Specifically, $\tilde{I}/\tilde{N}$ declines relatively slow when increasing the drug effectiveness initially until a critical level above which the prevalence begins to decline quickly. This indicates that relatively low treatment efficacy is not enough to effectively control the infectious disease. Compared with case 1) $p_1 = 40, p_2 = 50$, the same drug efficacy leads to a lower disease prevalence for the case 2). Furthermore, the threshold of disease elimination for drug efficacy also reduces from $\eta = 0.55$ to $\eta = 0.47$ in the absence of macro to micro coupling. This demonstrates that ignoring the impact of macro transmission dynamics on micro virus dynamics may underestimate

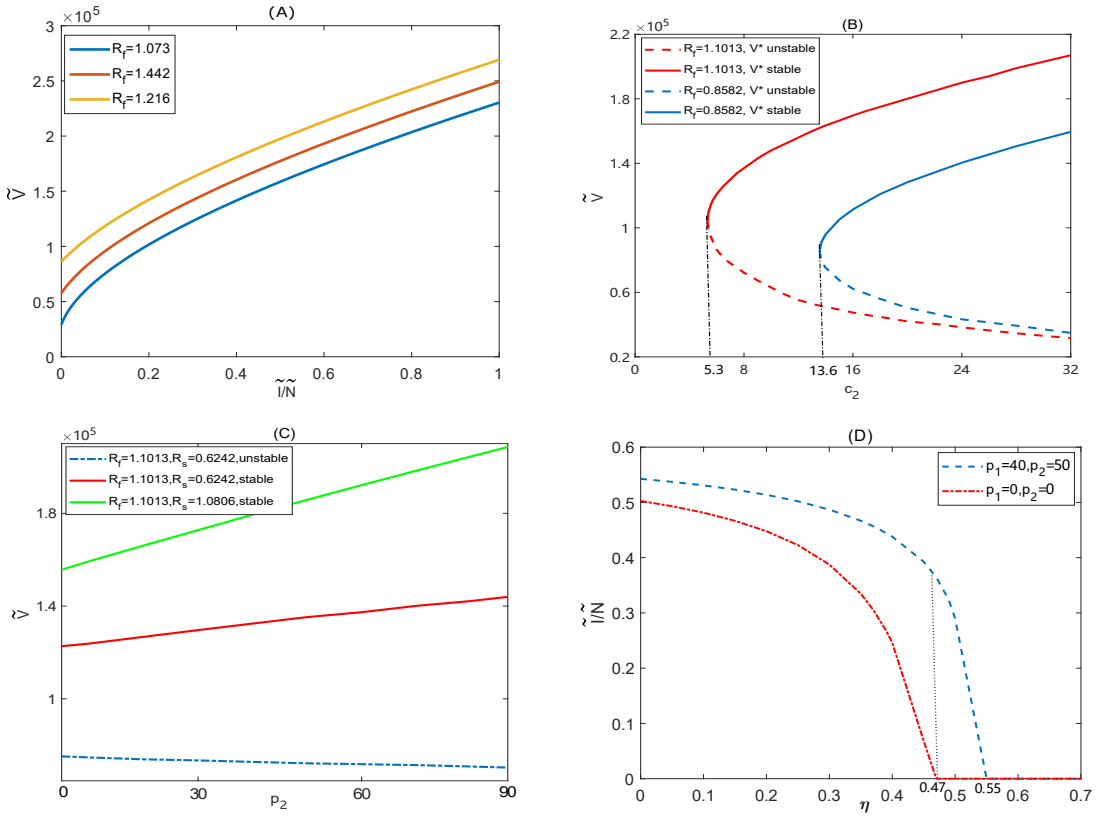

Figure 5. The interactions between macro dynamics and micro dynamics. The plot shows the variation of equilibrium $\tilde{V}$ against (A) the macro equilibrium $\tilde{I}/\tilde{N}$; (B) the contacts rate c_2 under two cases: $R_f > 1$ and $R_f < 1$; (C) the viral releasing rate per contact p_2 under two cases: $R_f > 1, R_s < 1$ and $R_f > 1, R_s > 1$; (D) the variation of prevalence at equilibrium $\tilde{I}/\tilde{N}$ versus effectiveness of treatment η under two cases: $p_1 = 40, p_2 = 50$ (macro dynamics is coupled to micro model) and $p_1 = p_2 = 0$ (macro dynamics is decoupled from micro model) with fixed parameter values and initial values.

the transmission of diseases in the population and consequently the requirement of drug effectiveness.

Generally, for controlling infectious disease, we should implement measures to reduce the basic reproduction number and consequently the new infections. In this model, we can easily observe that R_s decreases with the value of macro parameters a_i, c_i $(i = 1, 2)$ decreasing and the value of micro parameter η increasing . However, the existence of backward bifurcation makes the control and elimination of infectious diseases more complicated. To explore the interactions between microscale and macroscale with $R_s \leq R_{sc}$, we plot the trends of contact rate c_2, transmission coefficient a_1 and drug effectiveness η at surface $R_s = R_{sc}$ in Figure 6. If the values of these three parameters are below this surface (i.e., $R_s < R_{sc}$), then there is no positive equilibrium and the disease can die out. Otherwise, the disease may be persistent. Furthermore, Figure 6 shows that as η increases, the parameter region of (a_1, c_2) in which disease doesn't outbreak enlarges. This demonstrates with high drug efficacy, the control measures with relatively low intensity can still eliminate the disease. However, for small drug effectiveness η, in order to eliminate the disease, we should not only reduce the infection rate, but also keep the contact rate at a low level.

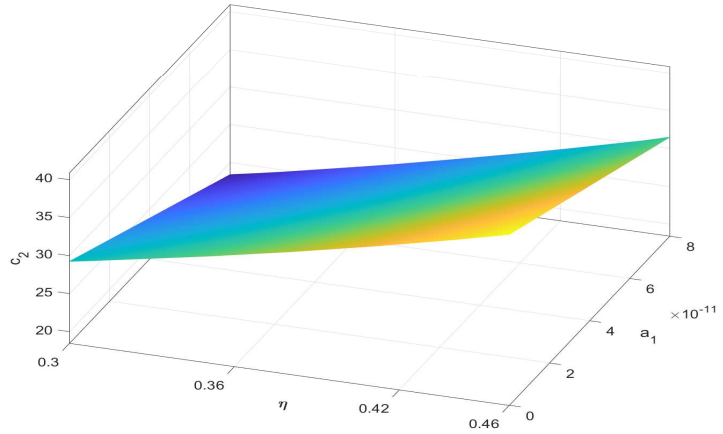

Figure 6. The 3-D plot shows the surface $R_s = R_{sc}$ against the contact rate c_2, transmission coefficient a_1 and drug effectiveness η. If these three parameters are below this surface, then $R_s < R_{sc}$, which means there is no positive equilibrium and the disease can be eradicated; Otherwise $R_s > R_{sc}$, the disease may be persistent.

6. Discussion

Multiscale systems can simultaneously describe the virus dynamics at the individual level and the transmission dynamics at the population level and have become a research focus in recent years. However, there are many challenges to constitute the linkage from the macroscale to the microscale. In this study, we formulate a multiscale model which can link the slow dynamics for disease transmission to the fast dynamics for viral progression, in order to examine the interactions of between-host dynamics and within-host viral dynamics. In fact, coupling the macro dynamics to micro models has been successfully proposed in environmentally driven infections. But, for some infectious disease such as HIV, the virus can be transmitted by direct contact with infected individuals, which may affect the generation rate of virus in microscopic level. Hence, in our model, the influx of viruses from infected individuals to the within-host system, depending on the contact rate and prevalence, becomes a bridge such that between-host dynamics is coupled to the within-host viral dynamics. What's more, the micro system is embedded into the macro system by introducing the viral load-dependent transmission rate and disease-induced mortality rate.

It is worth noting that the factors such as drug efficacy, individual differences and person-to-person contact influence the within-host dynamics, thereby affecting the value of viral load at the equilibrium, which in turn affects the spread of the disease at the population level. Therefore, it is extremely necessary to formulate a coupled model to reflect this feedback mechanism. Moreover, due to the fact that one can only contact a limited number of individuals per unit time, we choose the standard incidence instead of mass action in the model, which is a advantage compared with most existing coupled models. Of course, this also increases the difficulty of theoretical analysis.

We analyze the formulated model by studying the dynamics of the system on different time-scales, i.e., fast subsystem and slow subsystem. We prove that if $I > 0$, the within-host system globally converges to the unique positive equilibrium, which is independent on the threshold R_f obtained from the isolated microscopic model. For the slow subsystem, we find that the system can have zero, one or

two interior equilibria, which depends on the magnitudes of R_s and R_f. Specifically, for $R_s < 1, R_f > 1$ or $R_f < 1$, there exists a locally stable positive equilibrium and an unstable positive equilibrium. For $R_s > 1, R_f > 1$, there is only one locally stable interior equilibria. This demonstrates that the backward bifurcation may occur for the coupled system and $R_s = 1$ can not act as the threshold for infection control. Numerical simulations suggest that the full system exhibits the similar dynamic behaviors to the slow subsystem. For $R_s < 1, R_f > 1$ or $R_f < 1$, whether the disease dies out or persists depends on the initial condition.

We numerically examine the synergistic impact between the viral dynamics at the individual level and transmission dynamics at the population level. On the one hand, we observe increasing the drug effectiveness can decrease the prevalence of disease. Previous multiscale models that did not consider the impact of macroscale on microscale may overestimate the control effect of drug treatment on disease transmission. On the other hand, the contact rate may induce the occurrence of backward bifurcation and then affect the number and size of equilibria of viral dynamic model. Contact with infected individuals may cause the virus to persist in the population, even if the virus can not be persistent in the isolated individuals. This emphasizes limiting contact with infected individuals is effective in eliminating virus or controlling virus at a low level at the population level. The existence of backward bifurcation also illustrates the coupled system has more complicated dynamics, and consequently results in the elimination of disease more complex. The suggested control measures may include both the reduction in contact rates or transmission rate at the population level and the increase in drug efficacy at the individual level, and using these control measures together can effectively control the diseases.

In summary, we developed a novel bidirectional coupled model with standard incidence and investigated the synergistic impact between the macro transmission dynamics and micro virus dynamics, which is a advantage compared to most existing multiscale models. We derived some interesting results from this model. The coupled system may appear the backward bifurcation and Hopf bifurcation under certain conditions. Especially, contact rate or drug efficacy is essential to induce these complex dynamic behaviors. The conclusions improve our understanding for prevention and control of infectious disease, which can not be obtained from the pure between-host transmission or within-host viral dynamic models. However, due to the complexity of coupled system, it is challenging to include all progression and transmission routes of infection in the model while providing a complete theoretical analysis.

Although this article is mainly discussed in the context of HIV, the approaches we used are able to be applied more generally in other infectious diseases. Moreover, it should be noted we study the rich dynamics that may occur in our proposed model by theoretical analysis and numerical simulations. However, due to the lack of reliable information on parameter values such as p_1, p_2, our simulations remain more qualitative. For example, the critical level of contact rate c_2 with two positive equilibria may be larger than the real situation. Hence, it is necessary to further discuss the possible dynamic phenomena and the corresponding parameter region in practical application. We leave it for future work.

Acknowledgments

This work is supported by the National Natural Science Foundation of China (NSFC,11631012).

Conflict of interest

All authors declare no conflicts of interest in this paper.

References

1. R. M. Anderson, R. M. May, O. U. P. (OUP), *Infectious diseases of human: dynamics and control*, 1992.
2. O. Diekmann, J. Heesterbeek, Mathematical epidemiology of infectious diseases: Model building, analysis and interpretation, *Wiley Series in Mathematical and Computational Biology, Chichester, Wiley*.
3. A. S. Perelson, P. W. Nelson, Mathematical Analysis Of HIV-1 Dynamics In Vivo, *Siam. Rev.*, **41** (1999), 3–44.
4. P. Song, Y. Lou, Y. Xiao, A spatial seirs reaction-diffusion model in heterogeneous environment, *J. Differ. Equations*, **267** (2019), 5084–5114.
5. S. Wain-Hobson, Virus dynamics: Mathematical principles of immunology and virology, *Nat. Med.*, **410** (2001), 412–413.
6. L. J. Abu-Raddad, R. V. Barnabas, H. Janes, H. A. Weiss, J. G. Kublin, I. M. Longini, et al., Have the explosive HIV epidemics in sub-Saharan Africa been driven by higher community viral load?, *AIDS*, **27** (2013), 2494–2496.
7. D. Wilson, M. Law, A. E. Grulich, D. A. Cooper, J. M. Kaldor, Relation between HIV viral load and infectiousness: a model-based analysis, *The Lancet*, **372** (2008), 314–320.
8. T. C. Quinn, M. J. Wawer, N. Sewankambo, D. Serwadda, R. H. Gray, Viral load and heterosexual transmission of human immunodeficiency virus type 1, *New. Engl. J. Med.*, **342** (2000), 921–929.
9. L. M. Childs, F. E. Moustaid, Z. Gajewski, S. Kadelka, R. Nikinbeers, J. W. Smith, et al., Linked within-host and between-host models and data for infectious diseases: a systematic review, *PeerJ*, **7** (2019), e7057.
10. N. Dorratoltaj, R. Nikinbeers, S. M. Ciupe, S. Eubank, K. Abbas, Multi-scale immunoepidemiological modeling of within-host and between-host HIV dynamics: systematic review of mathematical models, *PeerJ*, **5** (2017), e3877.
11. A. Gandolfi, A. Pugliese, C. Sinisgalli, Epidemic dynamics and host immune response: a nested approach, *J. Math. Biol.*, **70** (2015), 399–435.
12. W. Garira, A primer on multiscale modelling of infectious disease systems, *Infect. Dis. Model.*, **3** (2018), 176–191.
13. W. Garira, A complete categorization of multiscale models of infectious disease systems, *J. Biol. Dyn.*, **11** (2017), 378–435.
14. M. A. Gilchrist, D. Coombs, Evolution of virulence: Interdependence, constraints, and selection using nested models, *Theor. Popul. Biol.*, **69** (2006), 145–153.
15. M. Park, C. Loverdo, S. J. Schreiber, J. O. Lloydsmith, Multiple scales of selection influence the evolutionary emergence of novel pathogens, *Philos. T. R. Soc. B.*, **368** (2013), 20120333.

16. M. Shen, Y. Xiao, L. Rong, Global stability of an infection-age structured HIV-1 model linking within-host and between-host dynamics, *Math. Biosci.*, **263** (2015), 37–50.
17. M. Shen, Y. Xiao, L. Rong, L. A. Meyers, Conflict and accord of optimal treatment strategies for HIV infection within and between hosts, *Math. Biosci.*, **309** (2019), 107–117.
18. M. Shen, Y. Xiao, L. Rong, G. Zhuang, Global dynamics and cost-effectiveness analysis of HIV pre-exposure prophylaxis and structured treatment interruptions based on a multi-scale model, *Appl. Math. Model.*, **75** (2019), 162–200.
19. Z. Feng, X. Cen, Y. Zhao, J. Velasco-Hernandez, Coupled within-host and between-host dynamics and evolution of virulence, *Math. Biosci.*, **270** (2015), 204–212.
20. Z. Feng, J. Velasco-Hernandez, B. Tapia-Santos, A mathematical model for coupling within-host and between-host dynamics in an environmentally-driven infectious disease, *Math. Biosci.*, **241** (2013), 49–55.
21. X. Wang, S. Tang, A multiscale model on hospital infections coupling macro and micro dynamics, *Commun. Nonlinear. Sci.*, **50** (2017), 256–270.
22. X. Sun, Y. Xiao, Multiscale system for environmentally-driven infectious disease with threshold control strategy, *Int. J. Bifurcat. Chaos*, **28** (2018), 1850064.
23. Y. Xiao, C. Xiang, R. Cheke, S. Tang, Coupling the macroscale to the microscale in a spatiotemporal context to examine effects of spatial diffusion on disease transmission, *B. Math. Biol.*, **82** (2020), 1–27.
24. S. Bhattacharya, M. Martcheva, An immuno-eco-epidemiological model of competition, *J. Biol. Dyn.*, **10** (2016), 314–341.
25. T. Kostova, Persistence of viral infections on the population level explained by an immunoepidemiological model, *Math. Biosci.*, **206** (2007), 309–319.
26. E. C. Manda, F. Chirove, Modelling coupled within host and population dynamics of and HIV infection, *J. Math. Biol.*, **76** (2018), 1123–1158.
27. X. Cen, Z. Feng, Y. Zhao, Emerging disease dynamics in a model coupling within-host and between-host systems, *J. Theor. Biol.*, **361** (2014), 141–151.
28. B. Boldin, O. Diekmann, Superinfections can induce evolutionarily stable coexistence of pathogens, *J. Math. Biol.*, **56** (2008), 635–672.
29. P. Dreessche, J. Watmough, Reproduction numbers and sub-threshold endemic equilibria for compartmental models of disease transmission, *Math. Biosci.*, **180** (2002), 29–48.